Stabilization through precipitation in a system of colloidal iron(III) pyrophosphate salts

Y. Mikal van Leeuwen [a,*], Krassimir P. Velikov [b,c], Willem K. Kegel [a,*]

[a] Utrecht University, Van't Hoff Laboratory for Physical and Colloidal Chemistry, Padualaan 8, 3584 CH Utrecht, The Netherlands
[b] Unilever Research and Development Vlaardingen, Olivier van Noortlaan 120, 3133 AT Vlaardingen, The Netherlands
[c] Utrecht University, Soft Condensed Matter Group, Princetonplein 1, 3584 CC Utrecht, The Netherlands

ARTICLE INFO

ABSTRACT

The ionic strength of a solution decreases during the precipitation of an insoluble salt, which can cause an initially unstable colloidal system to stabilize during its formation. We show this effect in the precipitation and aging of colloidal iron(III) pyrophosphate, where we observe two distinct stages in the aggregation process. The first stage is the formation of nanoparticles that immediately aggregate into clusters with sizes on the order of 200 nm. In the second stage these clusters slowly grow in size but remain in dispersion for days, even months for dialyzed systems. Eventually these clusters become macroscopically large and sediment out of dispersion. Noting the clear instability of the nanoparticles, it is interesting to find two stages in their aggregation even without the use of additives such as surface active molecules. This is explained by accounting for the rapid decrease of ionic strength during precipitation, rendering the nanoparticles relatively stable when precipitation is complete. Calculating the interaction potentials for this scenario we find good agreement with the experimental observations. These results indicate that coupling of ionic strength to aggregation state can be significant and should be taken into account when considering colloidal stability of insoluble salts.

1. Introduction

Pyrophosphate (diphosphate, $P_2O_7^{4-}$ or PP_i) is part of the biological energy cycle and DNA synthesis: it is released upon hydrolysis of adenosine triphosphate (ATP) to adenosine monophosphate (AMP): $ATP \rightarrow AMP + PP_i$ [1]. In combination with most multivalent cations, pyrophosphates form insoluble complexes in water [2–4] and their role as ligands has been widely studied [5,6]. Metal pyrophosphate salts are known for their chemical and structural complexity [7] and wide industrial [8–10] and biomedical [11,12] applications. As iron(III) pyrophosphate (ferric pyrophosphate, $FePP_i$) is one of the few iron compounds without color, it is commercially available as a food additive and mineral supplement. It is an easily concealable material and useful for fighting iron deficiency because of its good bioaccessibility [13–15]. While the applications mentioned above can greatly benefit from a colloidal approach, especially the delivery of micronutrients and nutraceuticals [16], most studies focus on macroscopic crystals and bulk material.

In this work we present a systematic study of the stability of colloidal iron(III) pyrophosphate salts and observe two characteristic stages in the aging of the system. The first stage consists of the precipitation of small nanoparticles which immediately aggregate into larger clusters. In the second stage, these clusters slowly grow in size but form an intermediate colloidal system. Eventually they become macroscopically large and sediment out of dispersion. During this growth, no change is found on the nanoparticle scale. By calculating the interaction potentials at various ionic strengths we find that the experimental results can be explained by taking into account the decreasing ionic strength during precipitation.

2. Experimental methods

2.1. Materials

$FeCl_3 \cdot 6H_2O$ and $AlCl_3 \cdot 6H_2O$ were purchased from Sigma Aldrich, NaCl and $Na_4P_2O_7 \cdot 10H_2O$ from Merck and $Mg(NO_3)_2 \cdot 6H_2O$ from Acros. All chemicals were used as received.

2.2. Preparation

Colloidal particles of iron pyrophosphate were prepared by dissolving 0.857 mmol $FeCl_3$ in 50 ml water and adding this dropwise in about 15 min to 0.643 mmol $Na_4P_2O_7$ in 100 ml water while stirring in a 250 ml round bottom flask (rbf). In general, a turbid white

* Corresponding authors. Fax: +31 302533870.
   E-mail addresses: Y.M.vanleeuwen@uu.nl (Y.M. van Leeuwen), W.K.Kegel@uu.nl (W.K. Kegel).

dispersion forms during the addition of the final ~5 ml. For the concentration series, different concentrations of iron and pyrophosphate were used. All concentrations mentioned in this work refer to the concentration of iron(III) in the final volume. The ratio Fe:PP$_i$ used in the precipitation is always stoichiometric, 4:3. All solutions were prepared in water deionized by a Millipore Synergy water purification system. Dialysis experiments were performed using Spectra/Por 2 Dialysis Membrane, MWCO 12-14.000. In a typical dialysis experiment the dispersion is dialyzed for 12 days during which the water is changed six times. The dialysis medium reaches a stable conductivity of 2.7 μS/cm after changing the medium three times.

2.3. Analysis

Dynamic Light Scattering (DLS) and zeta potential (ZP) measurements were performed on a Malvern Instruments Zetasizer Nano series machine in backscatter mode at 25 °C with 5 min of equilibration time. The DLS measurements were performed in ten runs of 15 measurements per run yielding a size averaged over all ten runs and a standard deviation between the runs. The zeta potential measurements followed the same procedure but used ten runs of 50 measurements. For transmission electron microscopy (TEM), dispersions were diluted 10 times and dried on a copper grid prior to analysis using a Tecnai 12 electron microscope from FEI Company. This method is referred to as dry-TEM in this work. For cryo-TEM, one drop of unaltered dispersion was placed on a cryo-TEM grid and blotted for 1 s before being quenched in liquid ethane. Samples were stored in liquid nitrogen before being analyzed using a Tecnai 20 electron microscope.

3. Results and discussion

3.1. Characterization

3.1.1. Iron pyrophosphate

Fig. 1a depicts a typical dry-TEM image of an (dialyzed or non-dialyzed) FePP$_i$ dispersion, showing extended aggregates consisting of polydisperse particles of 20 nm on average, with attached networks of ~5 nm particles. Cryo-TEM analysis in Fig. 1b yields similar images with one main difference: many of the smaller 5 nm nanoparticles are present as individual particles. This indicates that while drying effects occur for the 5 nm particles during the dry-TEM preparation method, the 20 nm particles are mostly unaffected. As the preparation method can have a large effect on particle size and shape and colloidal stability, we have tried various
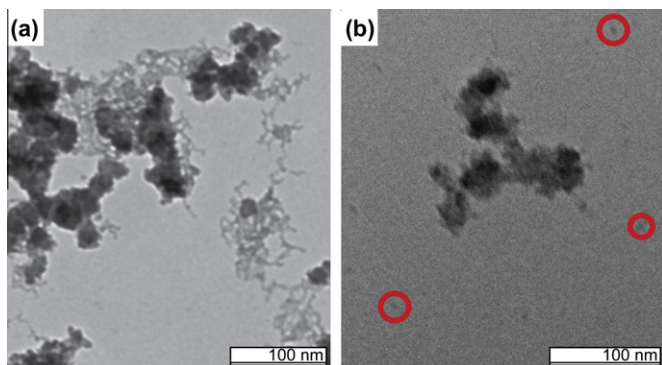

Fig. 1. TEM images of a non-dialyzed iron(III) pyrophosphate dispersion: comparison between Dry-TEM (a) and Cryo-TEM (b). The Cryo-TEM image shows a 100 nm aggregate with 5 nm smaller nanoparticles in the background, three of these are indicated with circles. Dialyzed dispersions yield similar images.
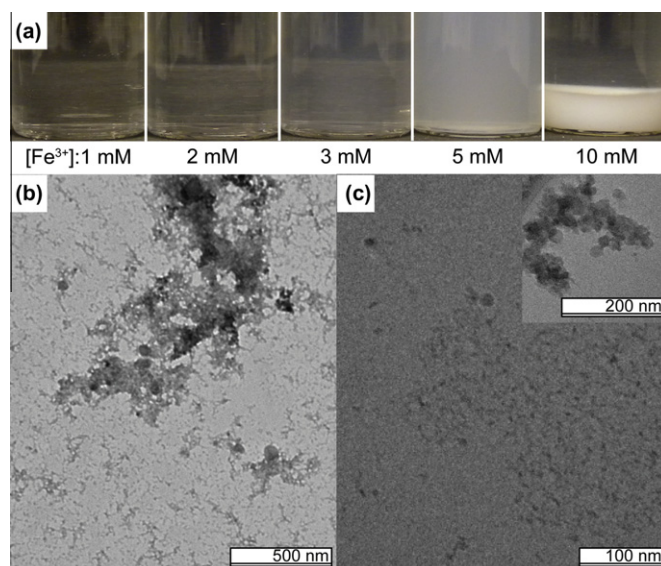

Fig. 2. The concentration range of iron(III) pyrophosphate (a) shows the precipitation limit to be around 2 mM Fe (see Section 3.1 for a definition). Dry-TEM (b) and cryo-TEM (c) images of the 2 mM Fe sample.

addition speeds and orders of addition. However, we have found little difference in particle morphology between methods as discussed in Supplementary material I.

3.1.2. Concentration

A concentration series ranging from 0.1 to 10 mM Fe was prepared. As mentioned in Section 2.2, concentrations refer to the concentration of iron(III) in the final volume, the ratio between Fe and PP$_i$ is always stoichiometric (4:3). The concentration in the standard procedure was 5.7 mM. Five of the samples around the precipitation limit are shown in Fig. 2a. From these samples the precipitation limit was estimated to be 2 mM: below this concentration the samples showed hardly any reflection when illuminated with a laser. DLS analysis of the dispersions from 2 to 5 mM shows cluster sizes similar to the standard concentration (5.7 mM) with a polydisperse particle size of 150 nm on average. Below 2.0 mM the noise levels become too high for DLS analysis. Both cryo- and dry-TEM images of the 2 mM sample show extended networks of small particles, see Fig. 2b and c. Aggregates of 20 nm particles are also observed as shown in the inset of Fig. 2c, but there are fewer present than at higher concentrations.

3.2. Cluster stability

When a non-dialyzed system is redispersed after having sedimented completely, subsequent sedimentation is noticeably faster. After several sedimentation and redispersion cycles it will even settle within minutes to hours depending on sample concentration and age. This observation is quantified by following the cluster size of a 5.7 mM system over time using DLS, see Fig. 3a. After about 24 days the aggregates in this dispersion became too large and polydisperse for the DLS measurements to be reliable. During this period, the cluster size in a dialyzed system remained stable at 200 nm. Comparing dry-TEM images of fresh dispersions (Fig. 1a) to those aged for 15 days (Fig. 3b), we find no significant difference in particle size or morphology. However, cryo-TEM images of aged samples show that the small, 5 nm subunits are now forming a network (Fig. 3c and d), while the aged dialyzed system shows no difference (not shown). The dialyzed system eventually also aggregates completely: after 6 months the cluster size has become
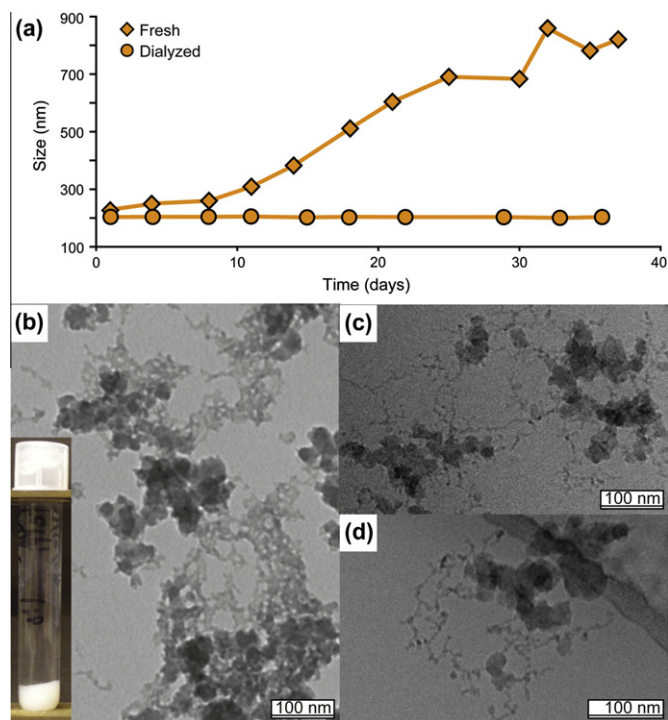
Fig. 3. (a) DLS analysis shows growth of the cluster size over time for the dialyzed (○) and non-dialyzed (◇) systems, while the TEM image (b) of the non-dialyzed system 15 days after preparation reveals no clear difference with the freshly prepared system. At this time the dispersion has sedimented completely (see inset). Cryo-TEM after 15 days (c) and 4 months (d) shows images similar to those in Fig. 1, but with the smaller 5 nm nanoparticles forming a network. Network formation was not observed for the dialyzed system.

too large for DLS analysis and the system cannot be redispersed anymore.

3.3. Effect of salt addition

We find that the addition of a fixed concentration of salt critically destabilizes a dialyzed system of $FePP_i$ and that this concentration varies with the valence of the added cation: 25 mM for Na^+, 0.45 mM for Mg^{2+} and 0.06 mM for Al^{3+}, see Fig. 4. From here on we will refer to this concentration as the critical coagulation concentration (ccc) [17]. The difference between regular sedimentation and a critically destabilized system can be seen in Fig. 4; the 0 mM sample in Fig. 4b is a freshly dialyzed system without any added salt, the 0 mM in Fig. 4a is 4 days after preparation. This illustrates the gradual sedimentation of a dialyzed system, while comparing the samples above and below the ccc shows the critical destabilization. The empirical Schulze–Hardy rule (SHR) states that the concentration of electrolyte needed to critically destabilize a colloidal dispersion inversely scales with ion valence to the power six [18]. Plotting the ccc's in a log–log fashion in Fig. 4d we find a slope of −5.5 (○), in close agreement with the SHR (red[1] line).

The results of DLS and zeta potential analyses of these dispersions are summarized in Table 1. DLS analysis of the Na^+ concentration range reflects the results of Fig. 4a: the sample at the ccc has a higher average cluster size and higher standard deviation. The Mg^{2+} and Al^{3+} samples show similar behavior slightly above the ccc. As can be seen from Table 1, the critical coagulation was not caused by reaching the iso-electric point of the particles since
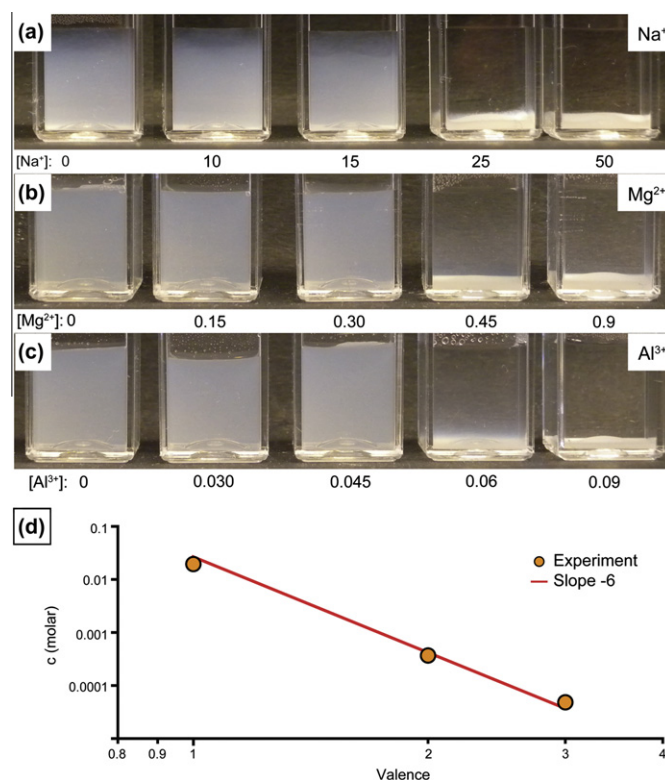
[1] For interpretation of color in Figs. 1–6, the reader is referred to the web version of this article.

Fig. 4. Critical coagulation of dialyzed $FePP_i$ dispersions 1 day after addition of several salts: NaCl (a), $Mg(NO_3)_2$ (b) and $AlCl_3$ (c). Concentrations in millimolar. 0 is the dialyzed dispersion without any added salt. Image (a) is taken 4 days after salt addition and shows further sedimentation of the concentrations below the ccc, illustrating the difference between regular sedimentation and rapid coagulation. Plotting the ccc's in a log–log fashion results in a slope of −5.5 (d), in close agreement with the SHR (solid line).

the zeta potential had not yet reached zero. The strong dependence of the zeta potential on the (concentration of the) added ion shown in Table 1 is a known effect for specifically adsorbing ions [17,19]. The negative zeta potential and the fact that it responds so strongly to addition of cations both indicate a negative surface charge of the $FePP_i$ particles.

3.4. Calculation of the interaction potential

As long as not all $FePP_i$ has precipitated, the ionic strength during precipitation is higher than just the NaCl counterion concentration of the final dispersion. Complete precipitation is defined here as the point at which the ionic strength of Fe^{3+} and PP_i^{4-} in solution is negligible: at the end of the precipitation process all material is present in the form of solid $FePP_i$ particles as the solubility of $FePP_i$ is very low. Therefore, the ionic strength

$$I = \frac{1}{2}\sum_{i=1}^{n} c_i Z_i^2$$

will only be 17 mM (Na^+ and Cl^-) at complete precipitation. At the start of the reaction an additional 5.7 mM Fe^{3+} and 4.3 mM PP_i^{4-} are present, resulting in an ionic strength of 77 mM. The initial concentration of Fe^{3+} is much higher than the ccc found for trivalent ions in Fig. 4, but will decrease during precipitation. We calculate the full interaction potential for the small (5 nm) and large (20 nm) nanoparticles at various concentrations of Fe^{3+} during the precipitation reaction to estimate particle stability, see Fig. 5 for results. In these calculations we used a Hamaker constant of 25 k_BT and a surface

Table 1
Cluster size and zeta potential depending on concentration of added ion.

Cation	Concentration (mM)		Size (nm)	St. dev.[a] (nm)	Zeta potential (mV)	St. dev.[b] (mV)
Dialyzed[c]	–		211	1.9	−51.2	0.9
Na$^+$	15		213	1.5	−45.0	5.74
	25	(ccc)	290	19	−42.3	15.9
Mg^{2+}	0.30		212	1.5	−19.6	0.15
	0.45	(ccc)	214	1.5	−18.8	0.12
	0.60		269	16	−18.3	0.35
Al^{3+}	0.045		220	1.2	−25.9	0.32
	0.060	(ccc)	246	2.4	−24.1	0.60
	0.090		2000	30	−19.3	0.15

[a] DLS measurements are performed in 10 runs with 15 measurements per run, the standard deviation is between runs. Note that this is not the standard deviation of the cluster size.

[b] Zeta potential measurements are performed in 10 runs of 50 measurements, the standard deviation is between runs. All samples are at pH 3.6.
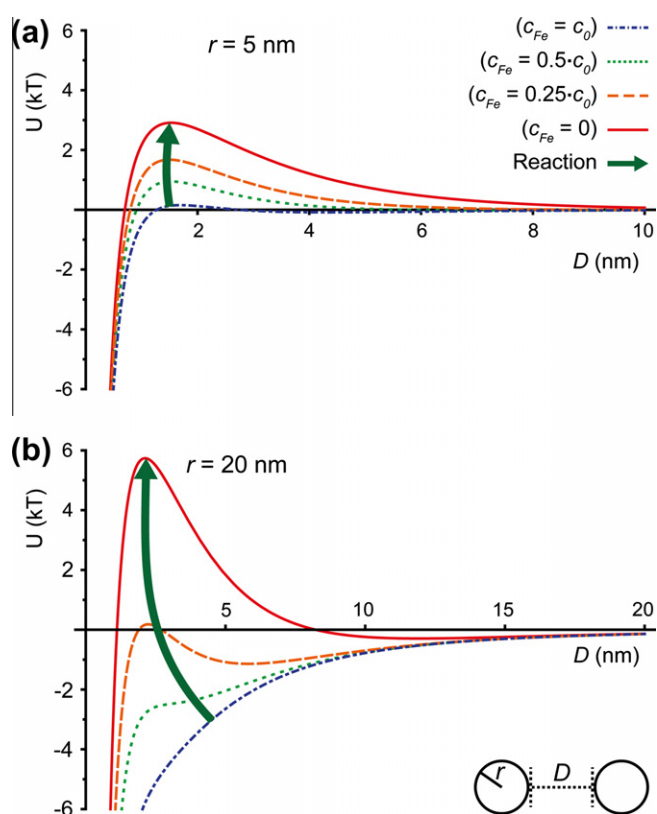
[c] Dialyzed system without any additional salt.

Fig. 5. Interaction potentials in k_BT of 5 nm (a) and 20 nm (b) particles at various concentrations of Fe^{3+} during the precipitation process. The concentration of iron in solution is labeled c_{Fe}, c_0 is the initial concentration at the start of the precipitation (5.7 mM). The thick arrows indicate the change in the potential during the course of the precipitation process.

potential of −45 mV, see Supplementary material II for details. We refer to the iron concentration as c_{Fe} and the initial iron concentration as c_0 (5.7 mM), the concentration of PP_i used in the calculations is always 3/4 that of iron. Note here that the potentials in Fig. 5 are expressed in the concentration of Fe^{3+} instead of the total ionic strength, but the calculations include all ions.

We find that at the start of the reaction both particle sizes are unstable since no (significant) stabilizing barrier is present in the interaction potentials (dash-dotted lines, $c_{Fe} = c_0$). When half of the $FePP_i$ has precipitated, the 5 nm particles have a stabilizing barrier of roughly 1 k_BT while the 20 nm particles are still unstable at this point (dotted lines, $c_{Fe} = 0.5 \cdot c_0$). For the 20 nm particles, the potential becomes only just positive when 3/4 of the $FePP_i$ has precipitated (dashed lines, $c_{Fe} = 0.25 \cdot c_0$). However, when precipitation is complete the stabilizing barrier is higher for the 20 nm particles than for the 5 nm particles (solid lines, $c_{Fe} = 0$).

3.5. Discussion

The experimental results show two stages in the aggregation process of the system. The first stage consists of the precipitation of nanoparticles and their immediate aggregation into 200 nm clusters. These clusters appear to be colloidally stable for long periods, illustrated by the presence of a ccc and the fact that the system obeys the Schulze–Hardy rule. However, the clusters slowly but continuously grow over time until they become too large to remain in dispersion. The calculated interaction potentials provide us with an explanation for these observations. Fig. 5 shows that the 20 nm particles initially are unstable and will aggregate while the 5 nm particles are kept relatively stable by the small energy barrier, as seen in Fig. 1. During precipitation the ionic strength of the solution decreases until the 20 nm particles also become stable, stopping further immediate aggregation and yielding finite (~200 nm) clusters in dispersion. The continuous further growth of these clusters could be caused by the formation of the networks of 5 nm particles shown in Fig. 3, which seems to occur on a similar timescale. As the final stabilizing barrier is relatively low for the 5 nm particles (~3 kT, see Fig. 5), these particles can slowly aggregate and connect the already existing larger clusters. This is confirmed by the fact that the dialyzed system remains stable for much longer periods, as the stabilizing barrier will be higher with the lowered ionic strength. The entire process is schematically summarized in Fig. 6. In this process we assume that the 5 nm particles will also aggregate with the 20 nm particles (especially in the early stages of the precipitation), or with 5 nm particles already attached to clusters of 20 nm particles, see Fig. 6 images 3 and 4.

While significantly larger, the clusters are not unlike the prenucleation clusters found for apatite (calcium phosphate). While Sommerdijk et al. study the formation of these clusters and crystals on templates, they also encounter the clusters in solution without any template present [20]. It is therefore possible that the formation and growth of $FePP_i$ is governed by similar principles: the 5 nm nanoparticles have grown from the prenucleation seeds and the 20 nm nanoparticles from the densification of the clusters in absence of a template. It would be interesting to see if crystallization of $FePP_i$ can be induced by performing the precipitation in the presence of a template, as colloidal $FePP_i$ always forms amorphous precipitates [21].

Having demonstrated that decreasing ionic strength during precipitation is the cause of the observed two stage precipitation, we
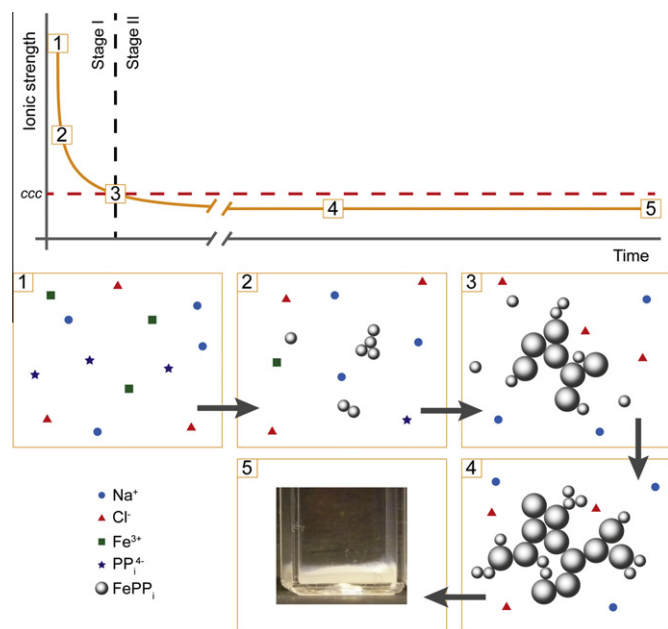
Fig. 6. Schematic representation of the precipitation and aging process. At the start of the reaction, all components are present as ions (1), which rapidly precipitate into small nanoparticles (2). The concentration of ions in solution is still above the *ccc* and therefore the nanoparticles aggregate, until most multivalent ions have precipitated and the formed clusters are stable on a short timescale (3). The smallest particles only have a weak stabilizing barrier which allows the clusters to slowly grow in time (4), until they are completely aggregated (5).

expect that this effect is general for the precipitation of insoluble salts. However, as the precipitating ions are multivalent in the case of FePP$_i$, this effect is amplified as these ions have a stronger effect on colloidal stability (see Fig. 4). When working with mono- and divalent ions it is likely that the concentration is below the *ccc* before and after precipitation and thus this effect will not be observed.

4. Conclusions

We have studied the colloidal system of iron(III) pyrophosphate and find two stages in its aggregation process. In the first stage small nanoparticles precipitate and immediately form clusters. In the second stage these clusters slowly grow over the course of days until they become macroscopically large and sediment out of dispersion. While the nanoparticle and aggregated states are common in most colloidal systems, the presence of this intermediate cluster stage is surprising regarding the instability of the nanoparticles. Our experimental observations are consistently explained by calculating the particle interaction potentials at various ionic

strengths. Taking into account that the ionic strength decreases during precipitation, we find that the nanoparticles are unstable at the start of the precipitation but form a stabilizing barrier in their interaction potential when precipitation is complete. These results explain both the immediate clustering of the nanoparticles and the slow further growth of the system. Finally, we have shown that the slow growth can be inhibited by dialysis. As this lowers the ionic strength even further, the stabilizing barrier increases and the system is kept from complete aggregation for periods of months.

Appendix A. Supplementary material

Supplementary data associated with this article can be found, in the online version, at http://dx.doi.org/10.1016/j.jcis.2012.05.018.

References

[1] B. Alberts, A. Johnson, J. Lewis, M. Radd, K. Roberts, P. Walter, Molecular Biology of the Cell, Garland Science, NY, New York, 1983.
[2] E. Hogfeldt, Stability Constants of Metal–Ion Complexes, The Chemical Society, London, 1964 (Special Publication No. 17).
[3] L.G. Sillen, A.E. Martell, Stability Constants of Metal–Ion Complexes, The Chemical Society, London, 1970 (Special Publication No. 25).
[4] L.G. Sillen, A.E. Martell, Stability Constants of Metal–Ion Complexes, The Chemical Society, London, 1964 (Special Publication no. 17).
[5] N. Shao, H. Wang, X. Gao, R. Yang, W. Chan, Anal. Chem. 82 (2010) 4628.
[6] Z. Guo, W. Zhu, H. Tian, Macromolecules 43 (2010) 739.
[7] J. Belkouch, L. Monceaux, E. Bordes, P. Courtine, Mater. Res. Bull. 30 (1995) 149.
[8] G.J. Hutchings, Appl. Catal. 72 (1991) 1.
[9] N.Y. Morozova, N.Y. Selivanova, Russ. J. Inorg. Chem. 21 (1976) 878.
[10] A. Ait Salah, P. Jozwiak, K. Zaghib, J. Garbarczyk, F. Gendron, A. Mauger, C.M. Julien, Spectrochim. Acta – Part A: Mol. Biomol. Spectrosc. 65 (2006) 1007.
[11] U. Gbureck, T. Hölzel, I. Biermann, J.E. Barralet, L.M. Grover, J. Mater. Sci.: Mater. Med. 19 (2008) 1559.
[12] A. Doat, F. Pellé, A. Lebugle, J. Solid State Chem. 178 (2005) 2354.
[13] R. Wegmüller, M.B. Zimmermann, D. Moretti, M. Arnold, W. Langhans, R.F. Hurrell, J. Nutr. 134 (2004) 3301.
[14] M.C. Fidler, T. Walczyk, L. Davidsson, C. Zeder, N. Sakaguchi, L.R. Juneja, R.F. Hurrell, Br. J. Nutr. 91 (2004) 107.
[15] F.M. Hilty, M. Arnold, M. Hilbe, A. Teleki, J.T.N. Knijnenburg, F. Ehrensperger, R.F. Hurrell, S.E. Pratsinis, W. Langhans, M.B. Zimmermann, Nat. Nanotechnol. 5 (2010) 374.
[16] K.P. Velikov, E. Pelan, Soft Matter 4 (2008) 1964.
[17] R.J. Hunter, Foundations of Colloid Science, Oxford University Press, 2001.
[18] E.J.W. Verwey, J.T.G. Overbeek, Theory of the Stability of Lyophobic Colloids, Dover Publications, Inc., 1999.
[19] E.E. Saka, C. Güler, Clay Miner. 41 (2006) 853.
[20] A. Dey, P.H.H. Bomans, F.A. Müller, J. Will, P.M. Frederik, G. De With, N.A.J.M. Sommerdijk, Nat. Mater. 9 (2010) 1010.
[21] Y.M. van Leeuwen, K.P. Velikov, W.K. Kegel, RSC Adv. 2 (2012) 2534.